

Sound velocity in shock compressed molybdenum obtained by *ab initio* molecular dynamics

T. Lukinov,¹ S. I. Simak,² and A. B. Belonoshko¹

¹*Department of Theoretical Physics, Condensed Matter Theory, AlbaNova University Center, Royal Institute of Technology (KTH), 106 91 Stockholm, Sweden*

²*Department of Physics, Chemistry and Biology (IFM), Linköping University, SE-58183 Linköping, Sweden*
(Received 17 May 2015; revised manuscript received 4 August 2015; published 24 August 2015)

The sound velocity of Mo along the Hugoniot adiabat is calculated from first principles using density-functional theory based molecular dynamics. These data are compared to the sound velocity as measured in recent experiments. The theoretical and experimental Hugoniot and sound velocities are in very good agreement up to pressures of 210 GPa and temperatures of 3700 K on the Hugoniot. However, above that point the experiment and theory diverge. This implies that Mo undergoes a phase transition at about the same point. Considering that the melting point of Mo is likely much higher at that pressure, the related change in the sound velocity in experiment can be ascribed to a solid-solid transition.

DOI: [10.1103/PhysRevB.92.060101](https://doi.org/10.1103/PhysRevB.92.060101)

PACS number(s): 64.10.+h, 64.70.K-, 71.15.Pd

On the basis of extensive experimental [1–11] and theoretical studies [12–32] of the phase diagram of Mo the following can be safely concluded. The body-centered cubic (bcc) phase of Mo is extremely stable up to very high pressures, at least in excess of 5 Mbars. Theory [26] predicts that, at a pressure of about 6.6 Mbars, Mo transforms to the double hexagonal close-packed structure. This result was recently independently confirmed by another theoretical study [31]. The high-temperature part of the Mo phase diagram remains controversial. There are two major experimental methods to assess the high-temperature part of the Mo phase diagram: the diamond-anvil cell (DAC) technique and the shock wave experiment. Early shock wave studies [5,7] revealed two discontinuities along the Hugoniot, one at the pressure of 2.1 Mbars and 4100 K (explained by a solid-solid transition) and another one at 4 Mbars and 9000 K (assigned to melting). The DAC studies [11] performed a few years later discovered nearly a flat melting curve for Mo. Being extrapolated, the DAC melting curve almost exactly matches the first discontinuity in the shock wave experiment. DAC studies never reached the conditions of the second discontinuity. Theory [23,24,27,28] has provided melting consistent with the shock wave data [5,8]. Somewhat similar patterns of studies emerged for a number of other metals (Ta [11,33–35] and Fe [36–40], e.g.) where theory and shock wave data on melting are in agreement whereas the DAC data demonstrate considerably lower melting temperatures. Considering that the latest DAC data on Fe and Ta support much higher melting T , it seems rather safe to conclude that the earlier DAC data were imprecise due to some yet unclear reasons. An explanation [41] suggested by one of the authors of this Rapid Communication is that the earlier DAC melting curves were in fact due to fast dynamic recrystallization induced by cumulative impact of increasing stress and softening of the sample either due to a solid-solid transition or simply due to an approach to melting. Indeed, first-principles calculations [23,24] pointed towards such a possibility in a number of metals. That, however, was objected to [28] on the grounds that the systems that provided the evidence for the existence of the solid-solid transition were either modeled using analytical potentials or were small when treated *ab initio*. We note, however, that the studies that did not support the existence of T -induced solid-solid

transitions are also performed for small systems [28]. It is, however, possible and even likely that such a transition is particularly sensitive to the size of the system. This is because the emerging phase is stabilized by the low-frequency thermal motion as, for example, is the case for the bcc Zr [42,43] and high-pressure bcc Fe [44]. A small system simply does not allow for the long wave oscillations since the small system cannot accommodate them. Yet, such oscillations are particularly important because they contribute significantly to the free energy and, thus, may stabilize the phase. Generally small systems favor the phase that is dynamically stable at low temperatures.

The recent shock wave experiment [8] that measured the speed of sound in the sample behind the shock wave front was expected to clarify this issue for Mo. However, the authors claimed that they did not see any discontinuity that could be assigned to a solid-solid transition, contrary to the previous shock wave experiment [5]. The authors do observe a peculiar behavior of the sound speed as a function of density, but that dependence was assigned to a particular behavior of the Mo bcc phase. Therefore, it is critical to compute the sound velocity of Mo in the bcc phase to verify whether indeed its sound velocity supports the hypothesis of the experimentalists.

First-principles calculations of Mo demonstrated that well-established data can be well reproduced with high precision. Equation of state, thermal expansion, crystal structure, and a broad pressure range of the bcc stability are in very good agreement with experimental data. The pressure-temperature-density ($PT\rho$) relation along the Hugoniot was also computed [29] in good agreement with experiment [5,7]. Therefore, it seems we can rely on the same approach to compute the sound velocity in the Mo bcc phase.

In order to do that, we performed a number of DFT based molecular dynamics (MD) calculations at the same densities as measured in the shock wave experiment.

The energies and forces were calculated within the framework of the frozen-core all-electron projector augmented-wave method [45] as implemented in the Vienna *ab initio* simulation package [46]. The energy cutoff was set to 350 eV. Exchange and correlation potentials were treated within the generalized gradient approximation [47]. The semicore $4p$ states of Mo were conservatively treated as valence. The finite tempera-

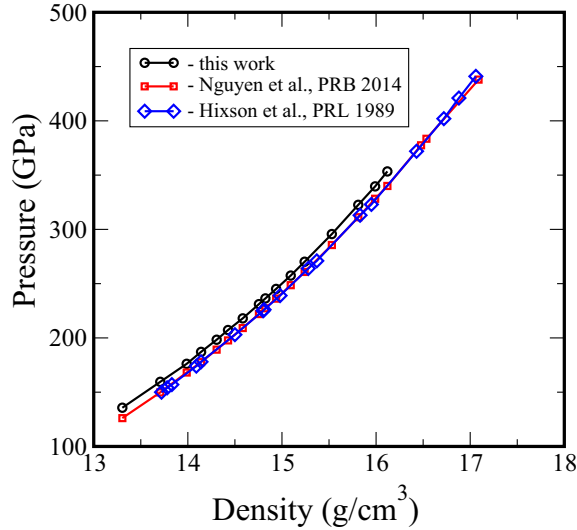


FIG. 1. (Color online) The calculated dependence of pressure on density along the Hugoniot compared to experimental data. The shift, independent of density, is typical of DFT calculations on metals.

tures for the electronic structure and force calculations were implemented within the Fermi-Dirac smearing approach [48]. All necessary convergence tests were performed, and the electronic steps converged within 0.01 meV/atom. The molecular dynamics runs have been performed in the canonical ensemble for a given volume and temperature. We used $5 \times 5 \times 5$ cubic supercells with 250 atoms. Tests have shown that the Γ point is sufficient at this size. The time step was set to 1 fs, and the runs continued for 4000 time steps. The averages were computed over the last 2000 and 1000 time steps, and the difference of these averages was considered as the error. This is probably a better estimate of the error than the statistical error that could be obtained by, e.g., a blocking technique. When a comparably short run is considered for a comparably small system, many factors contribute to the error, and such an estimate of the error is made in the spirit of computer experiments. The tests that have been performed for the cutoff of 500 eV and MD run duration of 8000 time steps confirmed convergence of the results regarding the cutoff and duration of MD runs (see the Appendix below). The computed pressures at the experimental densities and temperatures estimated in previous work [29] are compared with the pressures measured along the Hugoniot. A very reasonable agreement is obtained (Fig. 1). To estimate the sound velocity we need to compute elastic constants.

The single-crystal elastic constants were calculated via the generalized form of Hooke's law,

$$\sigma_i = c_{ij}\epsilon_j, \quad (1)$$

where σ_i stands for the stresses, c_{ij} stands for the elastic moduli, and ϵ_j stands for the strains; all in the Voigt notation ($i, j = 1, 2, \dots, 6$). The calculated time-averaged stresses associated with strains applied to our 250-atom supercell were used. To obtain the three nonzero c_{ij} 's of the cubic cells (namely, c_{11} , c_{12} , and c_{44}) just one deformation matrix is

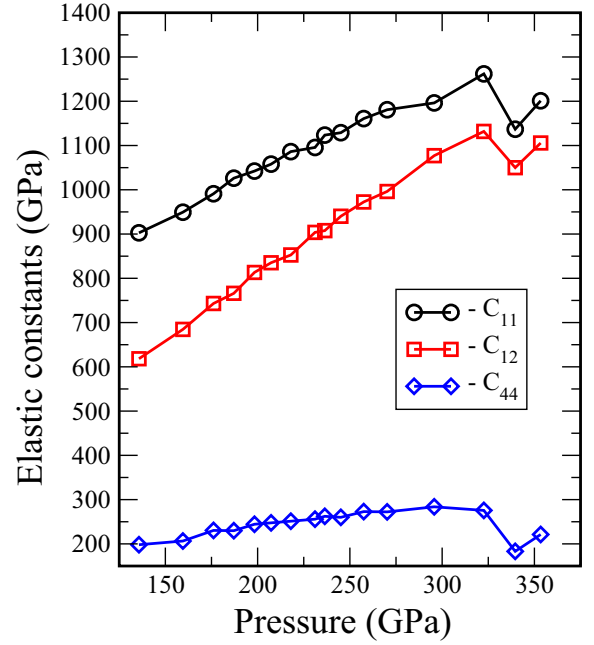


FIG. 2. (Color online) Elastic constants of bcc Mo along the Hugoniot as a function of pressure. The bcc phase of Mo becomes unstable above pressure 300 GPa which results in irregular behavior of elastic constants.

needed, whose components are shown below

$$\vec{\epsilon} = ([\delta, 0, 0, 0, 0, \delta]). \quad (2)$$

The applied δ 's were $\pm 2\%$ and $\pm 4\%$. The calculated dependencies of the time-averaged σ_i on δ were subject to a linear least-squares fit to directly estimate c_{ij} from the relations,

$$\sigma_1 = c_{11}\delta, \quad (3)$$

$$\sigma_2 = c_{12}\delta, \quad (4)$$

$$\sigma_6 = c_{44}\delta. \quad (5)$$

Figure 2 shows the pressure dependence of c_{11} , c_{12} , and c_{44} along the Hugoniot. Above the pressure of 325 GPa Mo the bcc phase becomes unstable for some deformations and melts. The sound velocity was computed in the Voigt-Reuss-Hill approximation [49]. The shear modulus G and the bulk modulus B of a cubic crystal can be written as

$$G = \frac{G_V + G_R}{2}, \quad (6)$$

$$B = \frac{C_{11} + 2C_{12}}{3}, \quad (7)$$

where

$$G_V = \frac{C_{11} - C_{12} + 3C_{44}}{5}, \quad (8)$$

$$G_R = \frac{5(C_{11} - C_{12})C_{44}}{4C_{44} + 3(C_{11} - C_{12})}. \quad (9)$$

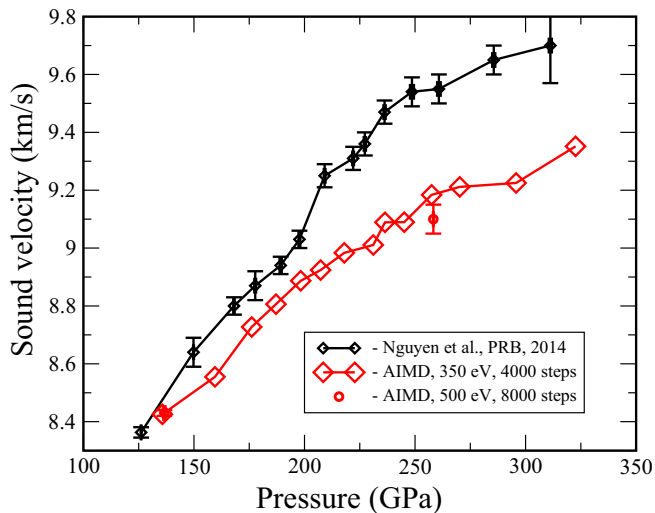


FIG. 3. (Color online) The calculated sound velocity (large diamonds) compared to experimental data (small diamonds with error bars). Up to the pressure of just above 200 GPa the experiment and theory provide very similar sound velocities (corresponding temperature is around 3700 K). At higher pressures the experiment and theory diverge, and it appears that the divergence increases with increasing pressure. The divergence cannot be explained by experimental error bars or statistical errors of our calculations. The size of the symbols corresponds approximately to the error bars. Somewhat irregular behavior of the experimental and theoretical curves also illuminates the possible error. The error bars of two computed points (circles with error bars) are obtained by the Monte Carlo method of error propagation with the errors in stresses obtained by the blocking technique (see the Appendix).

The longitudinal sound velocity C_L and the bulk sound velocity C_B can now be calculated as

$$C_L = \sqrt{\frac{(B + \frac{4G}{3})}{\rho}}, \quad (10)$$

$$C_B = \sqrt{\frac{B}{\rho}}. \quad (11)$$

Figure 3 provides the comparison of the recently measured sound velocity and the sound velocity calculated in this Rapid Communication. The agreement between experimental and theoretical data sets is very good, almost within mutual error bars up to pressures of just above 200 GPa and temperatures close to 4000 K, in fact, exactly where the discontinuity was found by Hixson and colleagues [5]. Above that pressure the experimental velocity goes sharply up, whereas the computed one smoothly continues the same trend as below the pressure 200 GPa. Above 325 GPa computed sound velocity exhibits erratic behavior (not shown) because the Mo crystal becomes unstable on smallest deformations. Such a change in experimental velocity might be possible if a new solid phase has emerged in the vicinity of 200 GPa. The discontinuity might not appear simply because the region behind the shock wave front might be inhomogeneous including both bcc and emerging phases that makes the transition comparably smooth. A very careful and improved experiment [8] has provided a

better resolution of the discontinuity, but the discontinuity seems to be there. A remote possibility is that something happens to the experimental setup in the vicinity of that point, but it has to have a similar impact both on the earlier experiment and on the recent one. Finally, something may happen to the accuracy of DFT calculations in that particular pressure-temperature range, but no obvious reasons, such as effects of strong electron correlations, can be named. Therefore we believe it is very unlikely. Thus, Mo does not seem to stay in the bcc phase up to the highest applied pressure. What is the nature of the emerging phase remains to be found out by truly large-scale DFT (or DFT-like precision methods) MD.

While this paper was in review, a Comment [50] and a Reply [51] were published where a peculiar behavior of the Mo shear modulus is discussed. It is also an indication that something happens to Mo in the experiment [8].

Computations were performed using the facilities at the Swedish National Infrastructure for Computing (SNIC). We also wish to thank the Swedish Research Council (VR) for financial support (Grants No. 2013-5767 and No. 2014-4750). S.I.S. acknowledges Linköping Linnaeus Initiative for Novel Functional Materials (LiLi-NFM) and the Swedish Government Strategic Research Area Grant in Materials Science Advanced Functional Materials (AFM). Comments by the anonymous referee have helped to improve the paper.

APPENDIX

There are quite a few obstacles that can contribute to the quality of computed data. In this Appendix, we check the cumulative impact of the energy cutoff, duration of our molecular dynamic runs, and the way of estimating numerical errors. Although most of the runs are performed with the cutoff of 350 eV for 4000 time steps, in this Appendix we report results of the runs performed with the cutoff of 500 eV for 8000 time steps. We are aware that 350 eV is already a very high cutoff. Converged properties have already been reported at the cutoff of 224.6 eV [28]. However, the referee requested to check for an even higher cutoff, so this is why we do it here.

Table I shows the average pressures computed over the same periods of time with different cutoffs for two densities. It is obvious that the use of 350 and 500 eV as a cutoff produces identical pressures. The average pressures computed with a 500-eV cutoff over a number of time intervals are compared to the pressures computed over the last 4000 time steps in the runs with 8000 time steps (Table II). The last column lists the errors obtained by a blocking technique [52]. The errors obtained in different ways are quite comparable. They cannot be identical due to their statistical nature. The reason why they are similar is simple. In the blocking technique the error becomes constant

TABLE I. Impact of cutoff on average pressure (GPa).

| Density (g/cm ³) | Cutoff | |
|------------------------------|----------|----------|
| | 350 (eV) | 500 (eV) |
| 13.304 | 135.712 | 136.129 |
| 15.094 | 257.791 | 258.289 |

TABLE II. Impact of duration of MD run on average pressure (GPa).

| Density (g/cm ³) | Steps | | |
|------------------------------|-----------|-----------|-----------|
| | 2000–4000 | 4000–6000 | 4000–8000 |
| 13.304 | 136.129 | 136.190 | 136.177 |
| 15.094 | 258.290 | 258.292 | 258.295 |

when the blocks are long enough to remove the correlation between the blocks. In solids it is normally dozens or hundreds of time steps. Clearly, if the error is computed over the blocks of 1000 time steps, their magnitude becomes similar to those computed by the blocking technique.

We note, however, that although the evaluation of statistical errors in pressure and stresses is a straightforward procedure, the errors in sound velocities are more difficult to estimate. To do that we use the Monte Carlo (MC) method of error propagation. That is, we vary the computed stresses within their statistical errors, compute elastic constants and then, finally, sound velocities (as outlined in the main text). The result of these calculations is shown in Fig. 4 where histograms of 10 000 MC attempts for two densities are shown. The error being very small at low density (about 0.01 km/s) becomes considerably larger at higher density (about 0.05 km/s).

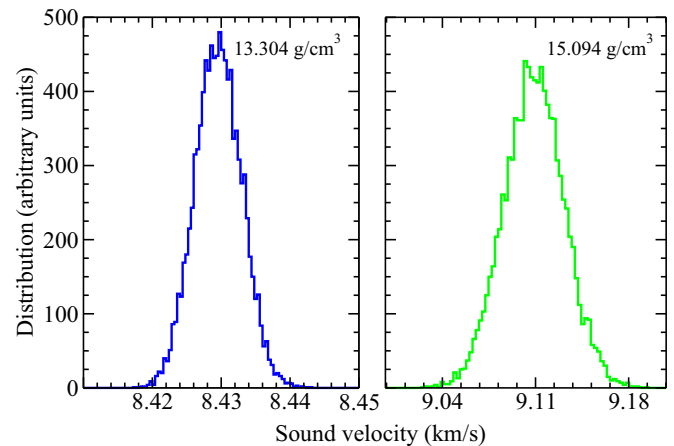


FIG. 4. (Color online) The histograms of longitudinal sound velocities computed at two densities as indicated in the legend. The width of the distribution represents the error in sound velocity. The error is larger at higher density that corresponds to the pressure of 257 GPa. The histograms are computed assuming errors in stresses computed by the blocking technique.

Yet, the errors are certainly small enough to see that the experimental and theoretical sound velocity curves are quite different above the pressure of 220 GPa.

- [1] J. M. Dickinson and P. E. Armstrong, *J. Appl. Phys.* **38**, 602 (1967); H. Wawra, *Z. Metallk.* **69**, 518 (1978).
- [2] N. S. Fateeva and L. F. Vereshchagin, *Pis'ma Zh. Eksp. Teor. Fiz.* **14**, 233 (1971) [*Sov. Phys. JETP Lett.* **14**, 153 (1971)].
- [3] J. M. Shaner, G. R. Gathers, and C. Minichino, *High Temp.-High Pressures* **9**, 331 (1977).
- [4] A. C. Mitchell and W. J. Nellis, *J. Appl. Phys.* **52**, 3363 (1981).
- [5] R. S. Hixson, D. A. Boness, J. W. Shaner, and J. A. Moriarty, *Phys. Rev. Lett.* **62**, 637 (1989).
- [6] Y. K. Vohra and A. L. Ruoff, *Phys. Rev. B* **42**, 8651 (1990).
- [7] R. S. Hixson and J. N. Fritz, *J. Appl. Phys.* **71**, 1721 (1992).
- [8] J. H. Nguyen, M. C. Akin, R. Chau, D. E. Fratanduono, W. P. Ambrose, O. V. Fat'yanov, P. D. Asimow, and N. C. Holmes, *Phys. Rev. B* **89**, 174109 (2014).
- [9] A. L. Ruoff, H. Xia, and Q. Xia, *Rev. Sci. Instrum.* **63**, 4342 (1992).
- [10] P. Oelhafen, R. Wahrenberg, and H. Stupp, *J. Phys.: Condens. Matter* **12**, A9 (2000); R. Wahrenberg *et al.*, *Europhys. Lett.* **49**, 782 (2000).
- [11] D. Errandonea, B. Schwager, R. Ditz, C. Gessmann, R. Boehler, and M. Ross, *Phys. Rev. B* **63**, 132104 (2001).
- [12] B. K. Godwal and R. Jeanloz, *Phys. Rev. B* **41**, 7440 (1990).
- [13] J. A. Moriarty, *Phys. Rev. B* **45**, 2004 (1992).
- [14] N. Singh, *Phys. Rev. B* **46**, 90 (1992).
- [15] S. M. Foiles, *Phys. Rev. B* **48**, 4287 (1993).
- [16] J. A. Moriarty, *Phys. Rev. B* **49**, 12431 (1994).
- [17] P. Söderlind, R. Ahuja, O. Eriksson, B. Johansson, and J. M. Wills, *Phys. Rev. B* **49**, 9365 (1994).
- [18] G. Davidov, D. Fuks, and S. Dorfman, *Phys. Rev. B* **51**, 13059 (1995).
- [19] N. E. Christensen, A. L. Ruoff, and C. O. Rodriguez, *Phys. Rev. B* **52**, 9121 (1995).
- [20] J. C. Boettger, *J. Phys.: Condens. Matter* **11**, 3237 (1999).
- [21] Y. Wang, D. Chen, and X. Zhang, *Phys. Rev. Lett.* **84**, 3220 (2000).
- [22] E. A. Smirnova, R. Ahuja, Yu. Kh. Vekilov, B. Johansson, Y. K. Vohra, and I. A. Abrikosov, *Phys. Rev. B* **66**, 024110 (2002).
- [23] A. B. Belonoshko, S. I. Simak, A. E. Kochetov, B. Johansson, L. Burakovsky, and D. L. Preston, *Phys. Rev. Lett.* **92**, 195701 (2004).
- [24] A. B. Belonoshko, L. Burakovsky, S. P. Chen, B. Johansson, A. S. Mikhaylushkin, D. L. Preston, S. I. Simak, and D. C. Swift, *Phys. Rev. Lett.* **100**, 135701 (2008).
- [25] C. Asker, A. B. Belonoshko, A. S. Mikhaylushkin, and I. A. Abrikosov, *Phys. Rev. B* **77**, 220102(R) (2008).
- [26] A. S. Mikhaylushkin, S. I. Simak, L. Burakovsky, S. P. Chen, B. Johansson, D. L. Preston, D. C. Swift, and A. B. Belonoshko, *Phys. Rev. Lett.* **101**, 049602 (2008).
- [27] C. Cazorla, M. J. Gillan, S. Taioli, and D. Alfé, *J. Chem. Phys.* **126**, 194502 (2007).
- [28] C. Cazorla, D. Alfé, and M. J. Gillan, *Phys. Rev. B* **85**, 064113 (2012).
- [29] C. Cazorla, M. J. Gillan, S. Taioli, and D. Alfé, *J. Phys.: Conf. Ser.* **121**, 012009 (2008).
- [30] A. K. Verma, R. S. Rao, and B. K. Godwal, *J. Phys.: Condens. Matter* **16**, 4799 (2004).
- [31] B. Wang, G. B. Zhang, and Y. X. Wang, *J. Alloys Compd.* **556**, 116 (2013).
- [32] O. M. Krasilnikov, M. P. Belov, A. V. Lugovskoy, I. Y. Mosyagin, and Y. K. Vekilov, *Comput. Mater. Sci.* **81**, 313 (2014).

- [33] L. Burakovsky, S. P. Chen, D. L. Preston, A. B. Belonoshko, A. Rosengren, A. S. Mikhaylushkin, S. I. Simak, and J. A. Moriarty, *Phys. Rev. Lett.* **104**, 255702 (2010).
- [34] J. M. Brown and J. W. Shaner, in *Shock Waves in Condensed Matter—1983*, edited by J. R. Asay *et al.* (Elsevier, Amsterdam, 1984), pp. 91–94.
- [35] A. Dewaele, M. Mezouar, N. Guignot, and P. Loubeyre, *Phys. Rev. Lett.* **104**, 255701 (2010).
- [36] J. M. Brown and B. G. McQueen, *J. Geophys. Res.* **91**, 7485 (1986).
- [37] A. B. Belonoshko and R. Ahuja, *Phys. Earth. Planet. Inter.* **102**, 171 (1997).
- [38] A. B. Belonoshko, R. Ahuja, and B. Johansson, *Phys. Rev. Lett.* **84**, 3638 (2000).
- [39] A. B. Belonoshko, R. Ahuja, and B. Johansson, *Nature (London)* **424**, 1032 (2003).
- [40] S. Anzellini, A. Dewaele, M. Mezouar, P. Loubeyre, and G. Morard, *Science* **340**, 464 (2013).
- [41] A. B. Belonoshko and L. S. Dubrovinsky, *Am. Mineral.* **81**, 303 (1996).
- [42] F. Willaime and C. Massobrio, *Phys. Rev. Lett.* **63**, 2244 (1989).
- [43] O. Hellman, I. A. Abrikosov, and S. I. Simak, *Phys. Rev. B* **84**, 180301(R) (2011).
- [44] A. B. Belonoshko, S. Arapan, and A. Rosengren, *J. Phys.: Condens. Matter* **23**, 485402 (2011).
- [45] P. E. Blöchl, *Phys. Rev. B* **50**, 17953 (1994); G. Kresse and D. Joubert, *ibid.* **59**, 1758 (1999).
- [46] G. Kresse and J. Hafner, *Phys. Rev. B* **48**, 13115 (1993); G. Kresse and J. Furthmüller, *Comput. Mater. Sci.* **6**, 15 (1996).
- [47] Y. Wang and J. P. Perdew, *Phys. Rev. B* **44**, 13298 (1991); J. P. Perdew, J. A. Chevary, S. H. Vosko, K. A. Jackson, M. R. Pederson, D. J. Singh, and C. Fiolhais, *ibid.* **46**, 6671 (1992).
- [48] N. D. Mermin, *Phys. Rev.* **137**, A1441 (1965).
- [49] R. Hill, *Proc. Phys. Soc., London, Sect. A* **65**, 349 (1952).
- [50] D. Errandonea, R. Boehler, and M. Ross, *Phys. Rev. B* **92**, 026101 (2015).
- [51] J. H. Nguyen, M. C. Akin, R. Chau, D. E. Fratanduono, W. P. Ambrose, O. V. Fat'yanov, P. D. Asimow, and N. C. Holmes, *Phys. Rev. B* **92**, 026102 (2015).
- [52] H. Flyvbjerg and H. G. Petersen, *J. Chem. Phys.* **91**, 461 (1989).